Journal of Nuclear Materials 389 (2009) 239–247

Contents lists available at ScienceDirect

Journal of Nuclear Materials

journal homepage: www.elsevier.com/locate/jnucmat

Nanoindentation on ion irradiated steels

P. Hosemann [a,b,*], C. Vieh [a,b], R.R. Greco [a], S. Kabra [a], J.A. Valdez [a], M.J. Cappiello [a], S.A. Maloy [a]

[a] Los Alamos National Laboratory, P.O. Box 1663, Los Alamos, NM 87544, USA
[b] Montanuniversität Leoben, Franz-Josef Strasse 18, 8700 Leoben, Austria

A B S T R A C T

Radiation induced mechanical property changes can cause major difficulties in designing systems operating in a radiation environment. Investigating these mechanical property changes in an irradiation environment is a costly and time consuming activity. Ion beam accelerator experiments have the advantage of allowing relatively fast and inexpensive materials irradiations without activating the sample but do in general not allow large beam penetration depth into the sample. In this study, the ferritic/martensitic steel HT-9 was processed and heat treated to produce one specimen with a large grained ferritic microstructure and further heat treated to form a second specimen with a fine tempered martensitic lath structure and exposed to an ion beam and tested after irradiation using nanoindentation to investigate the irradiation induced changes in mechanical properties. It is shown that the HT-9 in the ferritic heat treatment is more susceptible to irradiation hardening than HT-9 after the tempered martensitic heat treatment. Also at an irradiation temperature above 550 °C no detectable hardness increase due to irradiation was detected. The results are also compared to data from the literature gained from the fast flux test facility.

Published by Elsevier B.V.

1. Introduction

Ferritic/martensitic stainless steels have properties such as low swelling, low activation, resistance to embrittlement and hardening, and good corrosion resistance making them well suited for use in nuclear reactors and spallation targets [1]. It is believed that the BCC crystal structure and the fine lath microstructures are mainly responsible for the good properties under irradiation. To investigate the materials behavior under irradiation, mechanical tests on ferritic/martensitic steels irradiated in reactors or spallation sources have been performed in the past [2,3]. These tests are costly and increase the time needed to perform the tests. Moreover, the dose rate, the environment and temperature range are usually very limited in such experiments. A low energy proton beam can be used to induce displacement damage, [4,5] allowing for investigation of irradiation effects in materials without highly activating the specimens and thereby significantly reducing the costs for analysis. Due to the low energy of the protons, however, the proton penetration depth is limited. Therefore, nanoscale methods of testing irradiated materials need to be applied. Nanoindentation [6,7] is a small scale method which can be applied to investigate the changes of mechanical properties due to microstructural alteration from irradiation on the micron scale. In the present work, this method is applied to investigate the changes in the mechanical properties due to proton and alpha irradiation at different temperatures and beam conditions in a HT-9 type alloy heat treated to produce both a large grained ferritic and fine tempered martensitic lath microstructures.

2. Experiment

2.1. Material production, treatment and material verification

A heat of a HT-9 material was produced in a 25 kg vacuum furnace at the Montanuniversität Leoben in Austria. Table 1 presents the results of the chemical analysis performed. After casting the block (see Fig. 1), the material was hot forged at 1100 °C to about 30% strain in two directions and hot rolled at 900 °C to a thickness of 1.0 cm by Pittsburgh Materials Technology Incorporated. After hot rolling, the material was cold rolled and intermittently annealed at 760 °C numerous times down to a thickness of 1 mm. The resulting microstructure was large grained and ferritic (HT-9-F) (see optical micrograph in Fig. 1). A piece of the HT-9-F was then heat treated (normalized at 1050 °C for 1 h and air cooled and tempered at 760 °C for 1 h followed by AC) as shown in Fig. 1 resulting in a tempered martensitic microstructure (HT-9-M).

In order to confirm its ferritic crystal structure without retained austenite neutron diffraction was performed at the Lujan center at the Los Alamos Neutron Science Center (LANSCE) using the HIPPO diffractometer [8]. Neutron diffraction was performed on an 8 mm × 100 mm × 100 mm piece of HT-9-M material. The corresponding diffraction pattern is presented in Fig. 2. The resulting

* Corresponding author. Address: Los Alamos National Laboratory, P.O. Box 1663, Los Alamos, NM 87544, USA.
E-mail address: peterh@lanl.gov (P. Hosemann).

0022-3115/$ - see front matter Published by Elsevier B.V.
doi:10.1016/j.jnucmat.2009.02.026

Table 1
The nominal composition in wt% of the tested alloys.

Material	Fe	Cr	Mo	Si	C	Mn
HT-9	Bal.	11.95	1.0	0.4	0.2	0.6

peaks in the spectrum correspond with fully BCC Fe–Cr alloy. The red crosses in the figure represent actual neutron data while the green curve is the calculated diffraction pattern after a Rietveld refinement [8]. The difference curve (pink) shows that the calculated curve fits the data very well confirming that only the BCC phase is present.

2.2. Irradiations

Several different irradiations were conducted. Initial irradiations were performed using alpha particles. HT-9-M and HT-9-F were irradiated with 3.5 MeV He ions and analyzed using AFM and nanoindentation. The HT-9-M was irradiated using variable He energies to achieve a box like profile at different dose rates and analyzed using Nanoindentation followed by microstructural analysis using TEM. Next, a systematic experiment was conducted on HT-9-F and HT-9-M using a 900 keV proton beam at various temperatures. For each irradiation the NEC 9SDH-2 particle accelerator in the Ion Beam Materials Laboratory (IBML) at Los Alamos

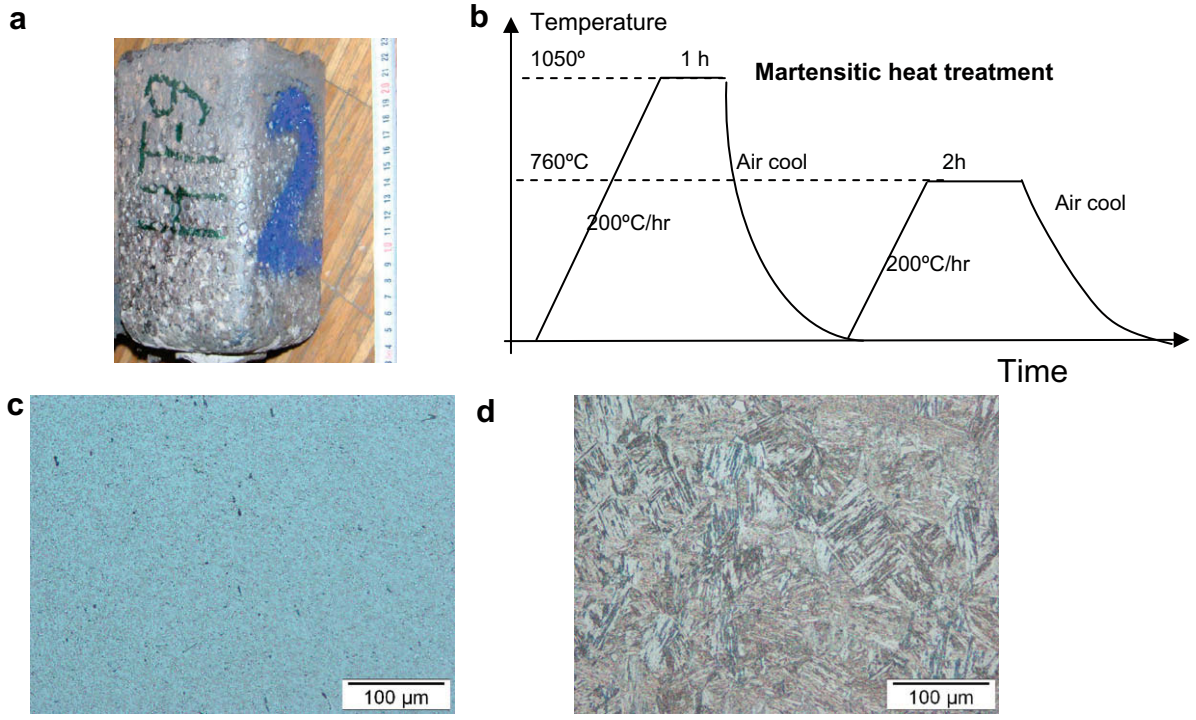

Fig. 1. Cast of HT-9 produced (a) and the heat treatment for martensite formation (b). (c) Optical micrographs of the as rolled material and the heat treated material (d).

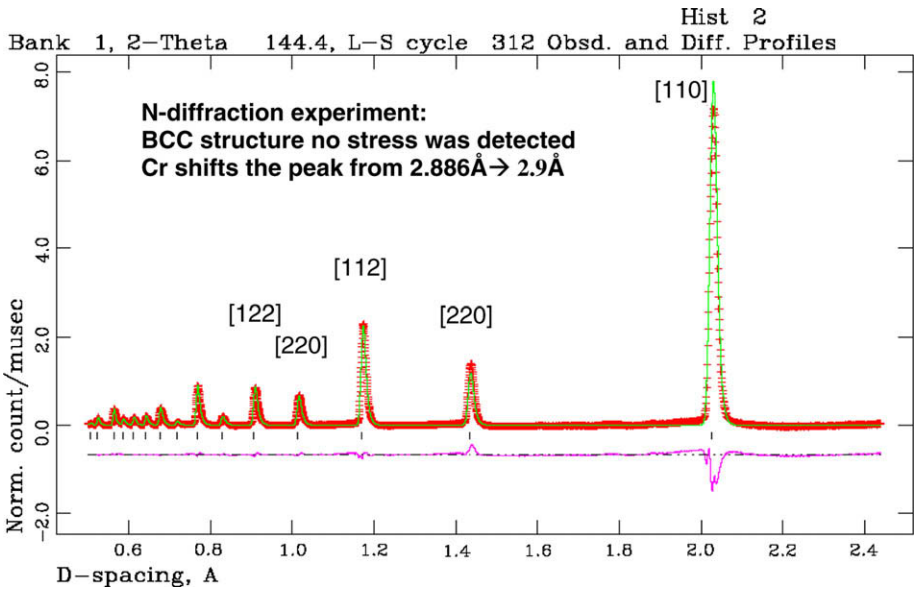

Fig. 2. Neutron diffraction spectrum on HT-9-M measured on the LUJAN center instrument HIPPO.

Table 2
Sample irradiation conditions.

Experiment	Material	Beam power	Dose	Temperature
He irradiation	HT-9-M	3.5 MeV	1.5–2	Room temperature
He dose rate	HT-9-M	2.25–3.25 MeV	1	Room temperature
Proton irradiation	HT-9-M HT-9-F	900 keV	0.5–1.5	Room temperature, 300 and 550 °C

National Laboratory (LANL) was used. The beam parameters and damage profile were calculated using SRIM 2006 [9]. Each irradiation experiment is described below in detail.

2.2.1. 3.5 MeV alpha irradiation (room temperature)

4 mm × 10 mm × 1 mm samples of the HT-9-F and HT-9-M materials were exposed to the 3.5 MeV alpha beam at the IBML at LANL using a current of 600 nA (see Table 2). The samples were mounted on a Cu sample holder using silver paste and carbon tape to ensure good thermal and electrical conductivity. Finite element (FEM) calculations considering the heat sink at the back of the sample were conducted to ensure that the energy deposited in the sample by the beam did not lead to significant heating in the sample. It was determined that the sample temperature increase did not exceed 5.2 °C. This leads to the assumption that even with poor thermal conductivity between sample and sample holder the beam heating is not significant. In addition the sample temperature was carefully monitored using K-type thermocouples mounted on the sample next to the beam spot during the experiment. The sample mounting is shown in Fig. 3. The beam location was determined using two sapphire scintillators. The two pieces of scintillators were mounted 2 mm apart from each other on top of the samples using double sided carbon tape. The set-up was designed so that four samples were irradiated simultaneously leaving a 1 mm × 1 mm area irradiated on each sample corner. Fig. 3 shows the sample stage for room temperature and high temperature irradiations. The beam current was monitored continuously during the experiment. The exact calculated dose profile is shown with the results in Fig. 4.

2.2.2. Alpha irradiation using variable beam power (room temperature) (dose rate experiment)

The HT-9-M specimens were irradiated using a He^+ beam with the energies 2.25, 2.5, 2.75, 3 and 3.25 MeV. The irradiation was started with the lowest energy of 2.25 MeV and ended with the highest energy of 3.25 MeV. This energy stepping created a box like damage profile as shown Fig. 4. The total charge and energy on each sample was collected with a Brookhaven Instrument Corporation current integrator. Additionally, a 100 V positive bias was applied to the sample to minimize electron loss from the samples for accurate current measurements. The peak helium concentrations in the sample found between 3 and 6 μm depth in the materials were calculated to be 2380 appm with a total charge of 4.8×10^{-4} coulombs (3×10^{15} particles) over a 4 mm^2 area. This fluence, 7.5×10^{16} He^+/cm^2 was determined using SRIM 2006 to produce ~1 displacement per atom (dpa) at the end of range for each irradiation energy. Three different dose rates were performed using the information above. The dose rates used were 1.54×10^{-4}, 7.41×10^{-5} and 6.02×10^{-5} dpa/s. Each sample was maintained at room temperature by mounting each sample on a substantial mass of copper (~0.5 kg) and insuring a good thermal contact with silver conductive adhesive. The sample temperature was monitored continuously during irradiation.

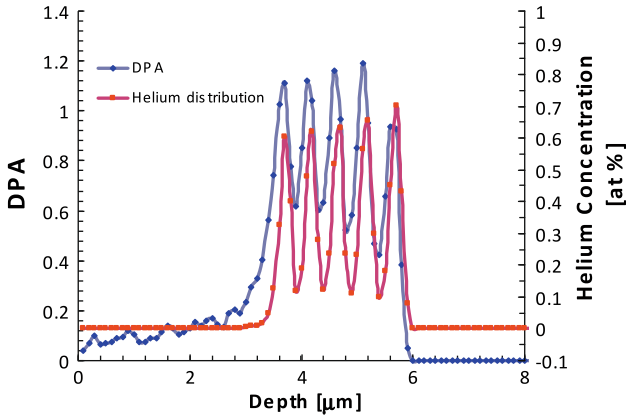

Fig. 4. Calculated dose and he concentration profile throughout the experiment with variable beam power.

2.2.3. 900 keV proton irradiation at different temperatures (room temperature, 300 and 550 °C)

HT-9-F and HT-9-M were irradiated at room temperature, 300 and 550 °C. The room temperature samples were mounted the same way as described above for the 3.5 MeV alpha beam experiment and in the literature [10].

The high temperature experiments were performed using a boron nitride heating stage equipped with a pyrolytic graphite boron nitride (PBN) heater having a heating capacity of 35 W/cm^2 and

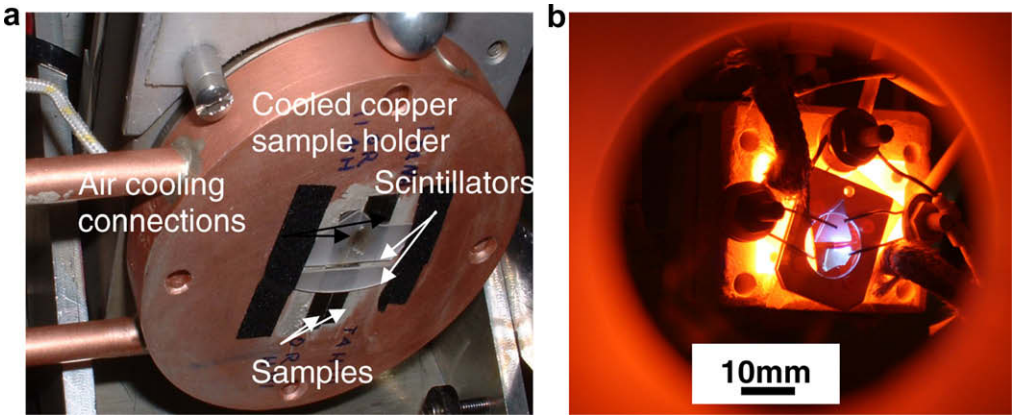

Fig. 3. Sample mounting in the ion beam accelerator in the room temperature experiment (a) and 550 °C experiment (b).

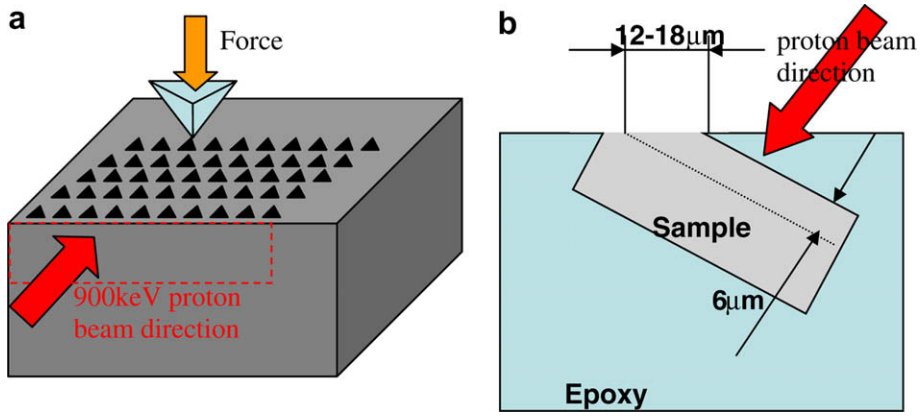

Fig. 5. Schematic sketch of the nanoindentation measurements (a). Schematic sketch of tilted sample mount (b).

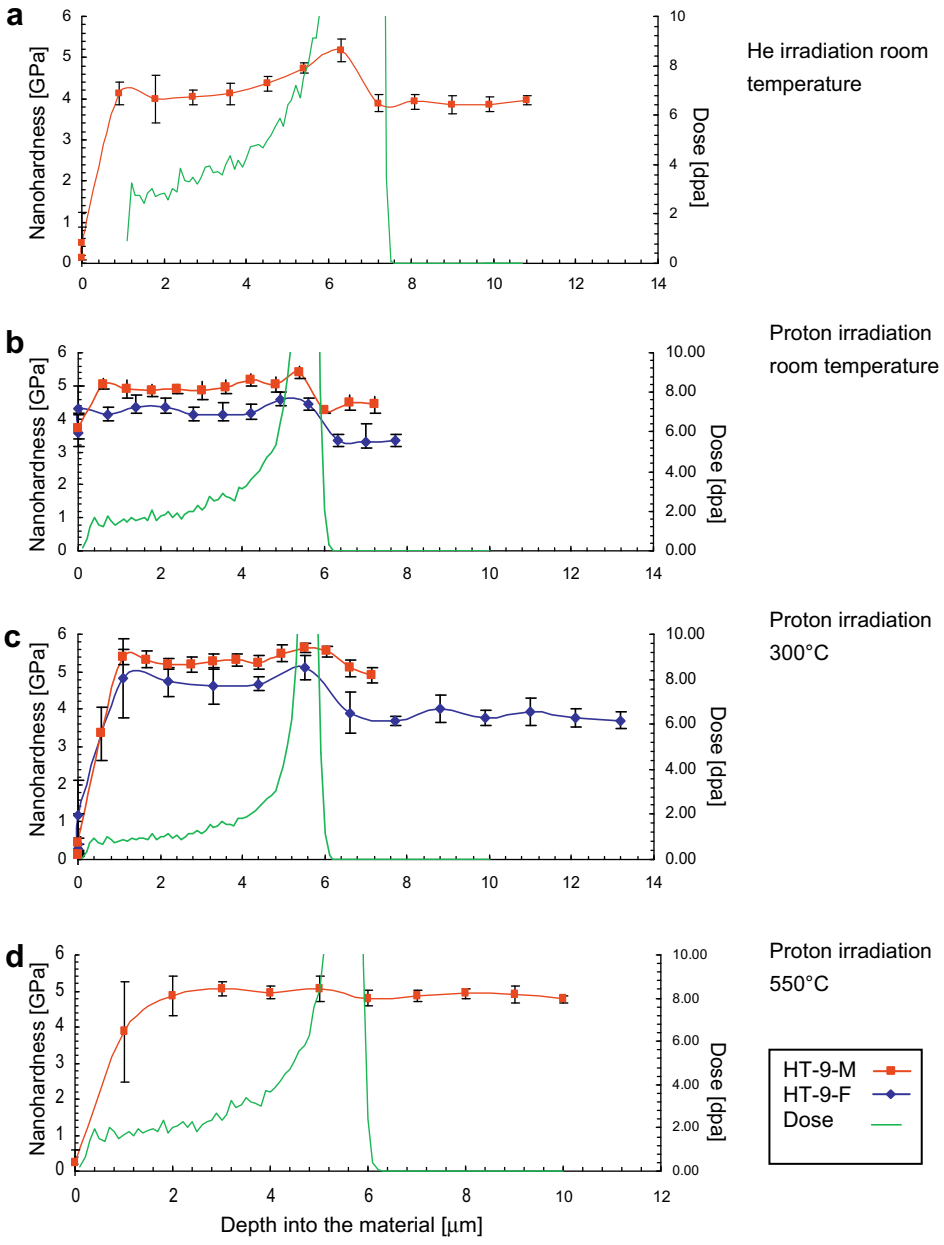

Fig. 6. Nanohardness results after He irradiation at room temperature (a), proton irradiation at room temperature (b), proton irradiation at 300 °C (c) and proton irradiation at 550 °C (d).

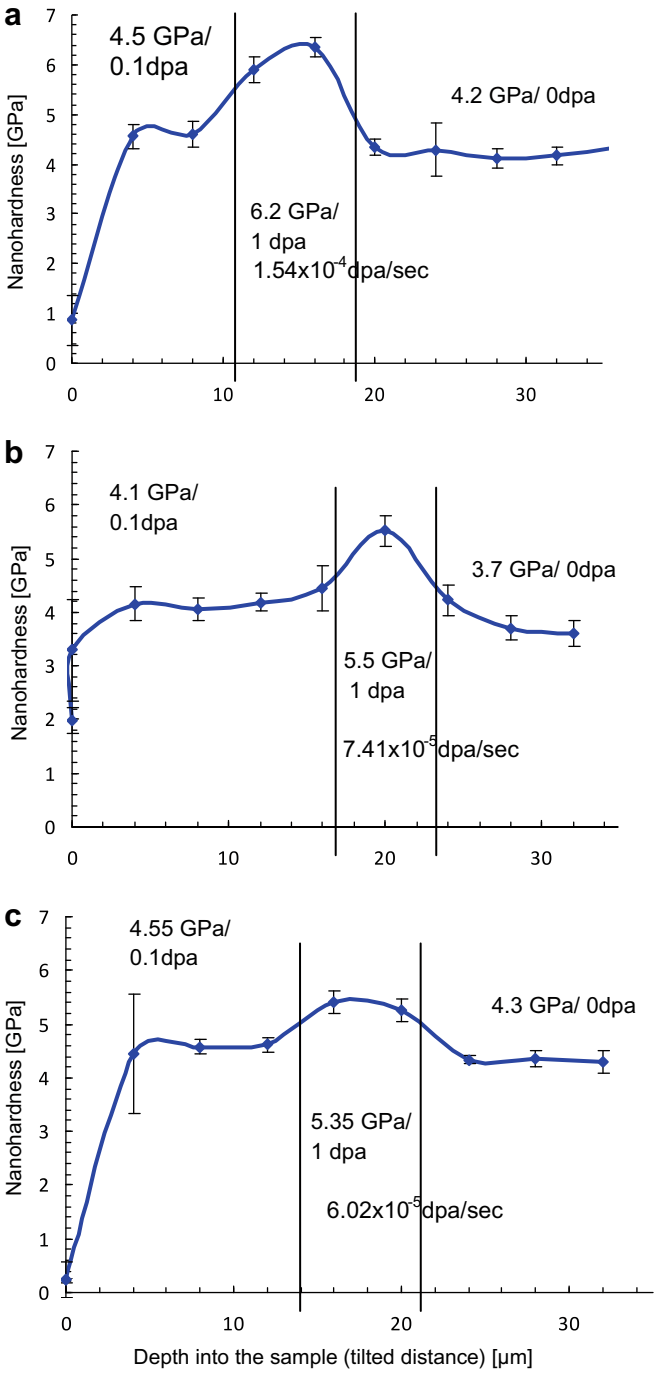

Fig. 7. Results of the cross section nanoindentation measurements on the He irradiated samples using different dose rates with variable beam energy (a) 6.02×10^{-5} dpa/s, (b) 7.41×10^{-5} dpa/s and (c) 1.5×10^{-4} dpa/s.

capable of 1500 °C in vacuum (Fig. 3(b)). During experimental set-up tests it was found that the decrease in electrical resistivity of the PBN with temperature does not allow a continuous beam current measurement. This necessitated including a 1 mm thick Al_2O_3 plate was used as additional electrical insulation and the beam was sampled every hour while turning off the power to the heater for 2–5 s. This allows a measurement of the beam current without leakage current artifacts from the heater. The average beam current was between 600 and 750 nA depending on the irradiation experiment. A 2×2 mm surface area irradiation (to ~1 dpa) took typically 30 h. The exact calculated dose profile is shown with the results in Fig. 4 for the He experiment and Figs. 8–11 for the proton experiments, respectively.

2.3. Nanoindentation, atomic force microscopy and transmission electron microscopy in cross section

After irradiation, all samples were analyzed in the same manner using nanoindentation. The samples were mounted in a 10–20° tilt towards the surface (Fig. 5) in epoxy cold mount by placing a piece of Cu with a certain thickness (depending on the sample size) underneath one edge of the sample to preserve the tilt angle until the epoxy hardens. After the epoxy was hardened the sample was polished with 0.05 μm colloidal silica as the last step on a Buehler vibromet polisher. The tilt increases the analyzing area by a factor of 2–5 depending on the tilt angle and therefore increases the hardness vs. depth resolution significantly compared to previous work [7]. The polishing provided a very flat and smooth surface as required for nanoindentation [7,10]. The nanoindenter used was a Hysitron Triboindenter® instrument equipped with a multi range nanoprobe, an optical microscope and an atomic force microscope (AFM). A Berkovich diamond indenter tip was used to perform the nanoindentation measurements. Starting from the edge, 14–18 rows with 8–10 indents in each row were placed parallel to the edge. This provided 8–10 indents at the same distance from the edge. The indents were 4 μm apart from each other. Constant displacement mode was used for all indents to ensure constant indentation depth. This eliminated the influence of the indentation size effect [11,12] within one array of indents. Before and after performing the array of indents, a contact mode AFM image using the indenter tip was scanned to ensure the location of the indents. After indentation, regular contact atomic force microscopy was performed using a silicon contact mode tip. The nanoindentation set-up and configuration are shown in Fig. 5.

After nanoindentation two samples were broken out of the epoxy mount to measure the tilt angle. Measuring the tilt angle ±1° by a 20° sample tilt leads to an uncertainty of ~1 μm on the surface. But the nanoindents have to be 4 μm apart from each other therefore the actually uncertainty by correlating the tilt angle to the maximum hardness increase is limited by the distance the indents are apart form each other. It was found that the region of the maximum hardness increase corresponds with the stopping peak of the sample within the uncertainty. Therefore the actual tilt angle was not measured on the remaining samples and the data were corrected by matching the maximum hardness increase area with the ion stopping peak in the sample.

The samples irradiated with alpha particles using variable beam energy were also investigated using transmission electron microscopy. The TEM samples were prepared using a FEI dual beam Focused Ion Beam instrument (FIB) [13]. The TEM used was a Philips CM 30. This general purpose TEM was used to perform electron diffraction analysis and conventional imaging. The TEM was operated using a LaB_6 filament. The sample stage allowed a ±45° specimen tilt and a point to point resolution of 0.23 nm. This analysis was performed to investigate localized damage from the beam stopping region.

3. Results

The pre irradiation experiments confirmed that the HT-9-M is purely BCC with lattice constants for a Fe–Cr alloy. No significant stress in the BCC lattice was detected. The metallography shows also that the HT-9-M has a tempered martensitic lath structure. Both measurements now allow one to state that the material contains a fine lath microstructure which is not is not highly stressed as observed in the martensitic crystal structure.

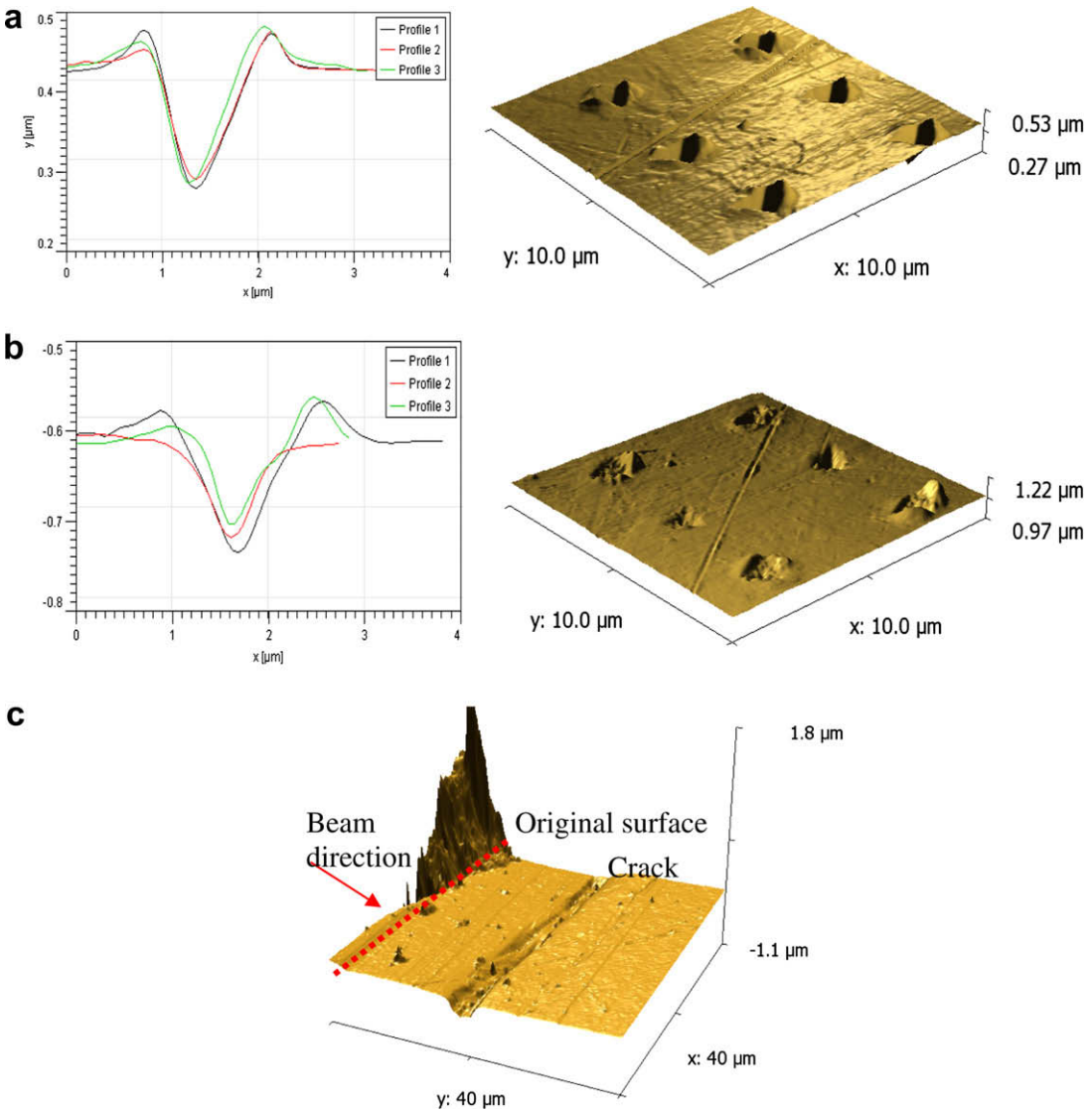

Fig. 8. AFM image and line scans of the nanoindent performed at the ion stopping region in the sample HT-9-M proton irradiation (a) and HT-9-M He irradiation (b) and the cracked region in HT-9-M he irradiated (c).

3.1. He irradiation at room temperature

The sample HT-9-M showed strong cracking approximately 17–18 µm deep parallel to the sample surface. Compensating for the 20° sample tilt, the cracks correspond with the He stopping peak region (Fig. 8(c)). At the location of the non cracked areas, nanoindentation measurements were performed. The He^+ stopping peak resulted in a significant hardness increase of 20–32 % relative to the unirradiated area deep in the sample (beyond the ion stopping peak). The 2 dpa irradiation region only showed a 3% hardness increase for HT-9-M (Fig. 6(a)). The trend of a slight hardness increase can be seen in the very first row of indents. This might be due to carbon deposition on the surface. AFM analysis after indentation showed that at the same depth where the cracks were found in the material (the He^+ stopping region), no pile up of material surrounding the nanoindents was also observed (Fig. 8(a)).

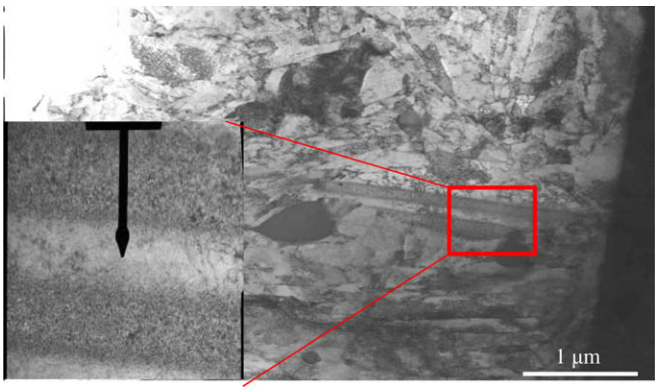

Fig. 9. TEM images of highest dpa rate, 1.054×10^{-4} dpa/s. (a) high magnification image of area of high defect density showing two stopping peaks and (b) beam direction is shown. The dark spot damage is clearly visible.

3.2. He dose rate irradiations

The nanoindentation results on all three specimens are shown in Fig. 7(a)–(c). It can be seen that the hardness increase follows the dose profile shown in Fig. 1 due to the ion irradiation. The tilting of the sample allows a high depth vs. hardness resolution so the ~3 µm wide implantation depth can be analyzed and 2–3 indents can be placed in that area. The three samples are not embedded in

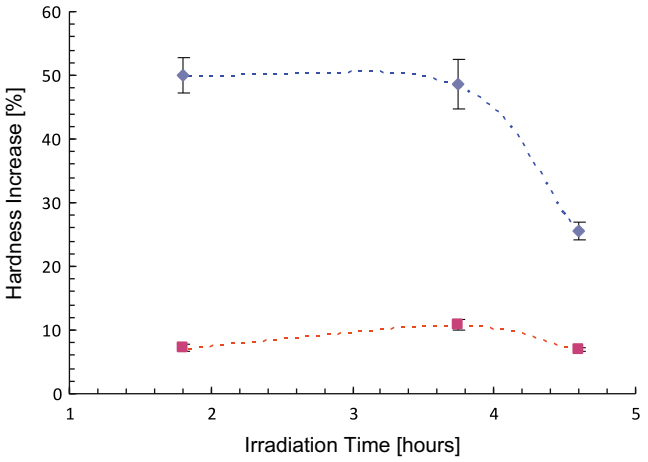

Fig. 10. Summary of the nanohardness results gained from the dose rate experiments for all three dose rates. Top curve is from helium implanted 'box-like' profile, bottom curve is measured at a shallow depth where the ion transported through the material.

the exact same angle. Therefore the irradiation depth vs. hardness profiles are slightly different. It can be seen in Fig. 4 that the dose and He concentration are not homogeneous throughout the implantation box. Each stopping peak is ~200 nm wide. Since the nanoindents are 1–1.5 μm wide it is believed that the hardness is an average hardness in that box type profile and not the hardness in between or on top of a stopping peak. A hardness increase due to the irradiation rate was found. It was found that the relative hardness increase (compared to the bulk material) was the highest for the fastest dpa rate sample $1.54 * 10^{-4}$ dpa/s) and the lowest for the low dpa rate sample ($6.02 * 10^{-5}$ dpa/s). It was also found that the area of homogeneous irradiation (before the stopping peak) showed a slight hardness increase of ~8–10%. No dose rate dependence was observed in this region.

3.3. Proton irradiation room temperature

Fig. 6 presents the hardness results gained from nanoindentation after proton irradiation to ~1 dpa. The 1 dpa region shows a clear hardness increase of 12% (for sample HT-9-M) and 24% (for the sample HT-9-F). The baseline for this calculation was the bulk unirradiated region. The ion stopping region shows a clear increase in hardness (~25–30%) relative to the surrounding area. The post indentation AFM revealed that no difference in pile up around the indentations could be detected when comparing indents in the stopping region to those in the bulk material.

3.4. Proton irradiation at 300 °C

The measurement shown in Fig. 6 revealed that the hardness increase in both materials is lower than what was measured in the room temperature experiment. The hardness increased 17% for the sample HT-9-F and 7% for the sample HT-9-M, respectively. Again the stopping peak region shows a hardness increase of 25–30% while no difference in pile up formation around the nanoindents in the stopping peak region was found.

3.5. Proton irradiation at 550 °C

At the 550 °C irradiation temperature the slight increase in the HT-9-M sample of average hardness is within the error bars. The HT-9-F material has not been investigated at this point.

4. Discussion

Performing nanoindentation in cross section allows measuring the hardness increase on samples with a high depth resolution. This allows measuring the hardness increase corresponding to a specific dpa value while hardness measurements from the surface will only give a hardness increase of averaged a dpa value. However, here in this publication all dpa values used in the text are the dpa values calculated in the sample depth of 2–4 μm so surface effects and stopping peak effects are not taken into account. In the following each experiment is discussed in detail and summarized and compared at the end.

4.1. He irradiation at room temperature

The cracks observed in the ion stopping range region of the sample and the different shape of the nanoindents (no pile up) in the stopping peak region allow one to state that this area is not representative for pure radiation damage. In contrast it can clearly be seen that the trapped He contributes to the hardness and changes the mechanical properties. Therefore using He to achieve high dose in short period of time can not be used successfully to gain information that compares to data obtained from high dose fission reactor irradiations.

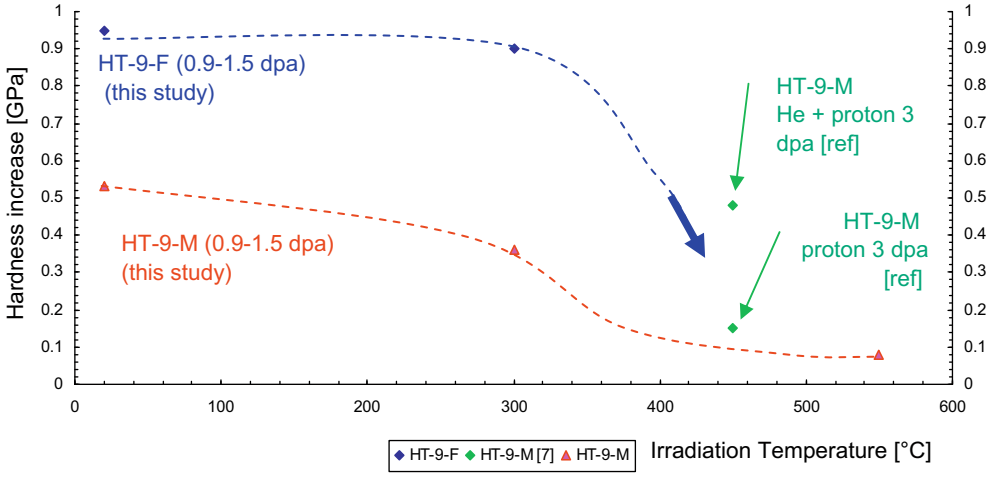

Fig. 11. Comparison of the irradiation data gained in this experiment compared to data gained previously.

4.2. He dose rate irradiations

The aim of this experiment was to use He ions to achieve extremely high dose rates. The comparison of data obtained at different dose rates (Fig. 7) show no significant difference measured in the low dose region where the He transports through the sample and higher hardness increase with higher dose rate in the stopping peak. According to Mansur [14,15] in order to compare lower dose rate experiments to higher dose rate experiments, the higher dose rate experiments has to be performed at higher temperature to allow for more recombination. Thus, since in this case all irradiations for the different dose rates were performed at the same temperature, it is understandable that the irradiations performed at a higher dose rate result in higher hardening. The shorter irradiation time for the higher dose rate sample allows less time for recombination of defects under irradiation resulting in the higher hardening observed in the higher dose rate sample.

The very distinct lines of black spot damage found by TEM indicate that almost no defect migration occurs during irradiation. But it is believed that the nanohardness measurements cannot distinguish the effects of this microstructure observed with TEM since the nanoindents have a width of $\sim$1 μm. These results suggest that it is not recommended to simulate fission reactor irradiation damage with this box type profile like experiment because of observed helium and dose rate effects.

4.3. Proton irradiations

The hardness measurements performed on the proton irradiations show that with higher irradiation temperature less hardening occurs as expected. The fact that the room temperature experiments were performed to 1.8 dpa while the higher temperature experiments were performed at 1 dpa might also play a small a role in the strong decrease in irradiation induced hardening observed at the higher temperature experiments. But it has been shown in the literature that the hardness difference between 1 and 1.8 dpa is minimal since above 0.5 dpa a gradual increase in mechanical properties is observed.

It appears that between the irradiation temperature of 300 and 550 °C, a strong hardness decrease occurs. Adding the literature data [7] as shown in Fig. 7 it can be seen that the decrease in irradiation induced hardness increase occurs between 450 and 550 °C. Previous work shows that in reactor experiments with a lower dose rate the transition temperature in radiation induced hardness increase is between 410 and 430 °C. It is known that irradiations with higher dose rate cause a shift in defect density (higher defects at high dose rate at the same irradiation temperature) and mechanical properties (more hardening at high dose rate at the same irradiation temperature) [14,15]. Considering this, the transition temperature from significant irradiation hardening due to the proton beam to almost no hardening are in the same temperature range than in [14,15].

An important result of the study shown here is that a clear difference can be seen in the ferritic and tempered martensitic material. It appears that the fine tempered martensitic microstructure has a significant effect in reducing hardening in HT-9. This can be explained by the fact that the martensitic microstructure which also contains carbides along these boundaries has a high density of interfaces which act as defect sinks for radiation induced defects.

4.4. General comments

All nanohardness measurements after irradiation clearly show a hardness change due to ion irradiation. In all cases the dose was calculated the same way using SRIM 2006. It is known that SRIM calculates the Vacancies/(ion $*$ Å) at 0 K and does not consider the difference in cascade shape and the recombination rate [16]. But in real experiments the samples are above 273 K and therefore the recombination plays a role. Also it is found in the literature that different ion species produce different cascade shapes [15]. Here it is stated that both play into the amount of defects remaining in the material and therefore into the remaining hardness. TEM analysis needs to be performed in order to investigate the remaining defect density after irradiation.

It is also found that the regions where the He ions stop show significant cracking and no pile up around the nanoindents while the region around the proton stopping region shows neither. It is postulated that this is the case because the He ions remain in the stopping region of the sample which increases the number of defects in that region while the protons are small enough to diffuse out of the material and only the dpa effect in that region remains. Considering all the different irradiation temperatures (room temperature, 300 and 550 °C), doses at the stopping peak (calculated 56 dpa for protons, calculated 179 dpa for He) and particles (He and protons) it was found that the hardness increase in the stopping region is always a maximum of 30% hardness increase relative to the bulk. This was the maximum increase in hardness that was found on these samples. This leaves the question why no higher hardness increase can be seen. This is most probably due to the fact that for materials irradiated to a dose above $\sim$1–2 dpa saturation in hardness (or strength) increase occurs and therefore not much additional hardening can be detected [15].

5. Conclusions

Based on this study on the irradiation effects on mechanical properties in ferritic/martensitic steels we have reached the following conclusions:

- Nanoindentation can be used to measure qualitative mechanical property changes due to ion irradiation. The location of the irradiated/ unirradiated interface can be accurately measured and agrees very well with the SRIM calculations. Even more the black spot damage observed using TEM can be found at the calculated depth.
- A tilted sample allows measuring the hardness increase in a sub micron level.
- The larger grained ferritic material hardens more under irradiation than the tempered martensitic material. This leads to a clear influence of microstructure on radiation induced hardening.
- The temperature transition where no or little hardness increase can be found due to irradiation is between $\sim$450 and 550 °C with these ion irradiation dose rates.
- It is not recommended to perform irradiation experiments using a box like profile with helium to achieve high dose faster. Many unaccountable effects can occur from the high concentration of helium and the higher dose rate which make a comparison of data to other irradiations more difficult.

Acknowledgements

This work was performed, in part, at the Center for Integrated Nanotechnologies, a US Department of Energy, Office of Basic Energy Sciences user facility. Los Alamos National Laboratory, an affirmative action equal opportunity employer, is operated by Los Alamos National Security, LLC, for the National Nuclear Security Administration of the US Department of Energy under Contract DE-AC52-06NA25396. The University of Leoben, and in particular Professor Gregor Mori and Professor Reinhard Pippan was supportive of this work by allowing an extensive student exchange.

We greatly appreciate the support of S. Vogel and Lujan Center at Los Alamos National Laboratory. This work has benefited from the use of the Lujan Neutron Scattering Center at LANSCE, which is funded by the U.S. Department of Energy's Office of Basic Energy Sciences. Los Alamos National Laboratory is operated by Los Alamos National Security LLC under DOE contract DE-AC52-06NA25396.

References

[1] D.S. Gelles, J. Nucl. Mater. 233 (1996) 293.
[2] Y. Dai, X. Jia, R. Thermer, D. Hamaguchi, K. Geissmann, E. Lehmann, H.P. Linder, M. James, F. Gröschel, W. Wagner, G.S. Bauer, J. Nucl. Mater. 343 (2005) 33.
[3] S.A. Maloy, T. Romero, M.R. James, Y. Dai, J. Nucl. Mater. 356 (2006) 56.
[4] G. Gupta, Z. Jiao, A.N. Ham, J.T. Busby, G.S. Was, J. Nucl. Mater. 351 (2006) 162.
[5] G.S. Was, J.T. Busby, T. Allen, E.A. Kenik, A. Jenssen, S.M. Bruemmer, J. Gan, A.D. Edwards, P.M. Scott, P.L. Andresen, J. Nucl. Mater. 300 (2002) 198.
[6] J.G. Swadener, E.P. George, G.M. Pharr, J. Mech. Phys. Solids 50 (2002) 681.
[7] P. Hosemann, J.G. Swadener, D. Kiener, G.S. Was, S.A. Maloy, N. Li, J. Nucl. Mater. 375 (2008) 135.
[8] S.C. Vogel, C. Hartig, L. Lutterotti, R.B. Von Dreele, H.R. Wenk, D.J. Williams, Pow. Diff. 19 (2004) 65.
[9] J.F. Ziegler, J.P. Biersack, The Stopping and Range of Ions in Matter, SRIM, 2006.
[10] P. Hosemann, S.A. Maloy, R.R. Greco, J.G. Swadener, T. Romero, J. Nucl. Mater. 384 (2009) 25.
[11] F. Schulz, H. Hanemann, Z. Fuer Metall. 33 (1941) Heft 3.
[12] W.D. Nix, H. Gao, J. Mech. Solids 46 (3) (1998) 411.
[13] D. Kiener, C. Motz, M. Rester, M. Jenko, G. Dehm, Mater. Sci. Eng. A 459 (2007) 262.
[14] L.K. Mansur, J. Nucl. Mater. 206 (1993) 306.
[15] G.Was, Fundamentals of Radiation Material Science, Springer, 2007. ISBN:978-3-540-49471-3..
[16] James F. Ziegler, Jochen P. Biersack, Matthias D. Ziegler, SRIM The Stopping and Range of Ions in Matter, 2008. ISBN:0-9654207-1-X.